Supplementary Information

Table S1 Selected bond lengths (Å) and bond angles (°) of Ni(II) and Co(II) centers in the compounds **1**and **2** respectively.

Bond distances of 1 (in Å)		Bond angles of 1 (in Degree)	
Ni1–O1W	2.047(2)	O1W–Ni1–O2W	90.12(9)
Ni1–O3W	2.0648(19)	O1W–Ni1–O4W	90.13(9)
Ni1–O4W	2.0743(19)	O1W–Ni1–O3W	175.46(8)
Ni1–O2W	2.0621(19)	O1W–Ni1–N1	88.67(8)
Ni1–N1	2.117(2)	O1W–Ni1–N9	89.18(8)
Ni1–N2	2.130(2)	O2W–Ni1–O4W	178.95(8)
O2W–Ni1–O3W	89.81(8)	O3W–Ni1–N1	86.80(8)
		O3W–Ni1–N9	95.35(8)
		O3W–Ni1–O4W	89.87(8)
		O2W–Ni1–N1	91.30(8)
		O2W–Ni1–N9	90.30(8)
		O4W–Ni1–N1	87.68(8)
		O4W–Ni1–N9	90.72(8)
		N1–Ni1–N9	177.32(9)
Bond distances of 2 (in Å)		Bond angles of 2 (in Degree)	
Co1–O1W	2.0792(14)	O1W–Co1–O1W#1	180.0
Co1–O1W#1	2.0792(14)	O1W–Co1–O1W#2	89.81(12)
Co1–O1W#2	2.0792(14)	O1W#1–Co1–O1W#2	90.19(12)
Co1–O1W#3	2.0792(14)	O1W–Co1–O1W#3	90.19(12)
Co1–N1	2.160(2)	O1W#1–Co1–O1W#3	89.81(12)
Co1–N1#1	2.160(2)	O1W#2–Co1–O1W#3	180.0
		O1W#3–Co1–N1#1	89.01(6)
		O1W–Co1–N1#1	90.99(6)
		O1W#2–Co1–N1#1	90.99(6)
		O1W#3–Co1–N1	90.99(6)
		O1W#1–Co1–N1	90.99(6)
		O1W#1–Co1–N1#1	89.01(6)
		O1W–Co1–N1	89.01(6)
		O1W#2–Co1–N1	89.01(6)
		N1–Co1–N1#1	180.0

#1 1-X, -Y, 1-Z; 2# 1-X, +Y, 1-Z; #3 +X, -Y, +Z.

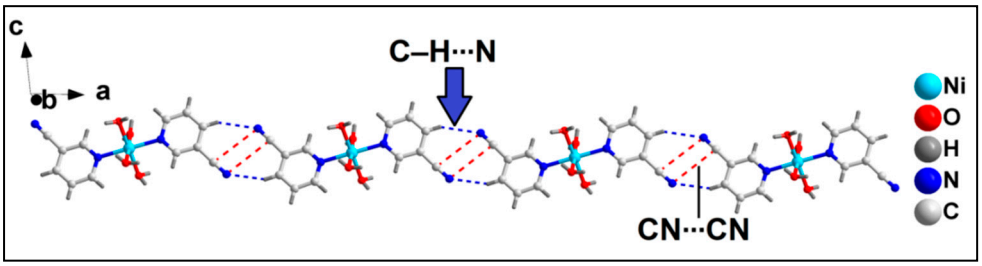

Figure S1. Formation of supramolecular 1D chain of compound **1** assisted by anti-parallel CN···CN and C–H···N hydrogen bonding interactions.

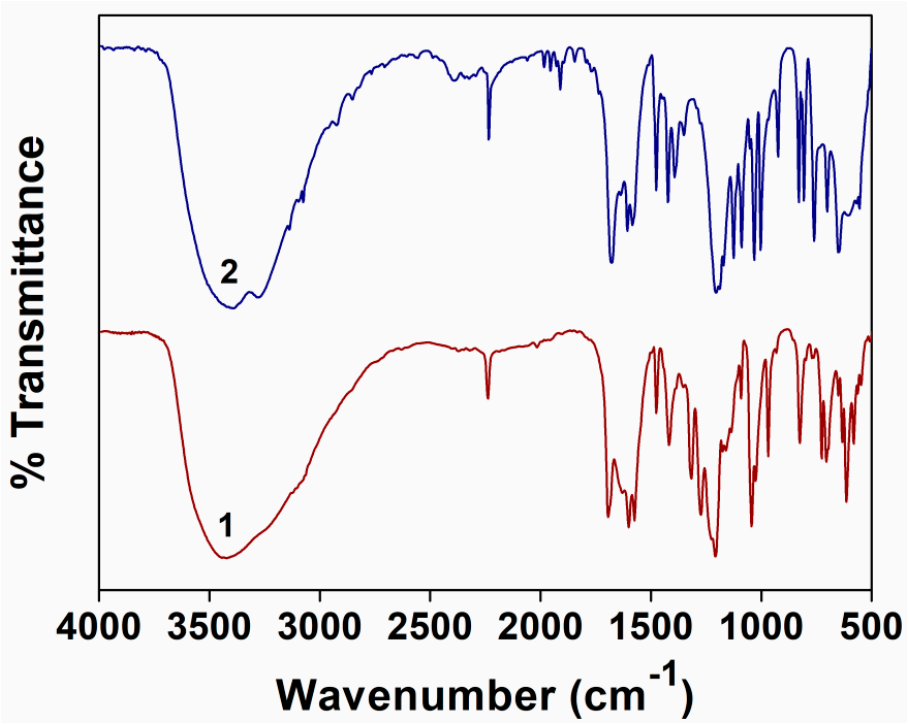

Figure S2. FT-IR spectra of compounds **1** and **2**.

3.3.2 Electronic spectroscopy

The UV-Vis-NIR spectrum of compound **1** shows three absorption bands (Figure S3) at 975, 662 and 380 nm [1]. The first spin-allowed transition, $^3A_{2g}\rightarrow{}^3T_{2g}(F)$ (ν_1), occurs at 975 nm. The electronic transition, $^3A_{2g}\rightarrow{}^3T_{1g}(F)$ (ν_2) gives rise to the 662 nm absorption band with a shoulder at 752 nm which may be a consequence of the transition from the $^3A_{2g}(F)$ to ^1E_g level, gaining intensity through a configuration interaction with the $^3T_{1g}(F)$ level, although some investigators prefer to interpret the doublet as arising from spin-orbit coupling [2]. The peak observed at 380 nm is due to the $^3A_{2g}\rightarrow{}^3T_{1g}(P)$ transition. The UV band originating from the $\pi\rightarrow\pi^*$ transition of the aromatic ligands is found at 271 nm [3-5]. The UV-Vis spectrum of **1** in water exhibits absorption bands at 286 nm. The absorption band at 385 nm can be assigned as $^3A_{2g}(F)\rightarrow{}^3T_{2g}(F)$ transition for octahedral Ni(II) ions and the bands at 663 nm with a shoulder at 756 nm can be assigned to $^3A_{2g}\rightarrow{}^3T_{1g}(P)$ transition.

The solid state UV-Vis-NIR spectrum (Figure S4) of compound **2** shows bands at 272 nm assigned to $\pi\rightarrow\pi^*$ transitions of the aromatic ligands [6,7]. Three ligand field bands *viz.* $^4T_{1g}(F)\rightarrow{}^4T_{2g}(F)$ (ν_1), $^4T_{1g}(F)\rightarrow{}^4A_{2g}(F)$ (ν_2) and $^4T_{1g}(F)\rightarrow{}^4T_{1g}(P)$ (ν_3) for the high-spin octahedral Co(II) complex for compound **2** are observed in solid state spectrum [8]. The first

band appears at 1251 nm, the third band is seen at 505 nm, and the ν_2 band due to $^4T_{1g}(F) \rightarrow {}^4A_{2g}(F)$ appears at 607 nm. However, the UV-Vis spectrum of compound **2** in aqueous phase (Figure S4b) shows weak absorption bands at 509 and 595 nm assigned to $^4T_{1g}(F) \rightarrow {}^4T_{1g}(P)$ (ν_3) and $^4T_{1g}(F) \rightarrow {}^4A_{2g}(F)$ (ν_2) transitions respectively. In the UV-Vis spectrum, the absorption bands corresponding to $\pi \rightarrow \pi^*$ transitions appear at 290 nm. Due to the limit of the wavelength window of the spectrophotometer used in this study, the NIR bands of the compounds are not seen in the aqueous phase spectra [9].

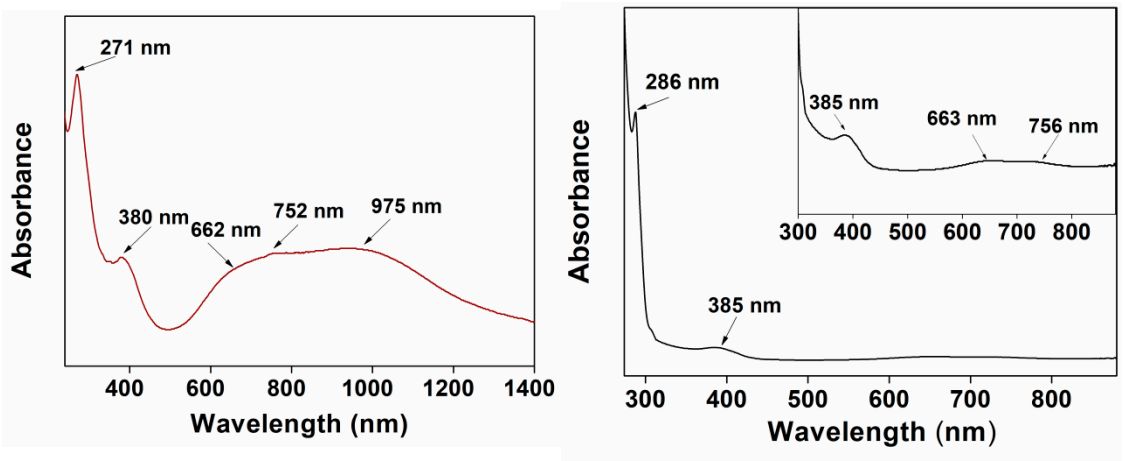

Figure S3. (**a**) UV-Vis-NIR spectrum of **1** (**b**) UV-Vis spectrum of **1**.

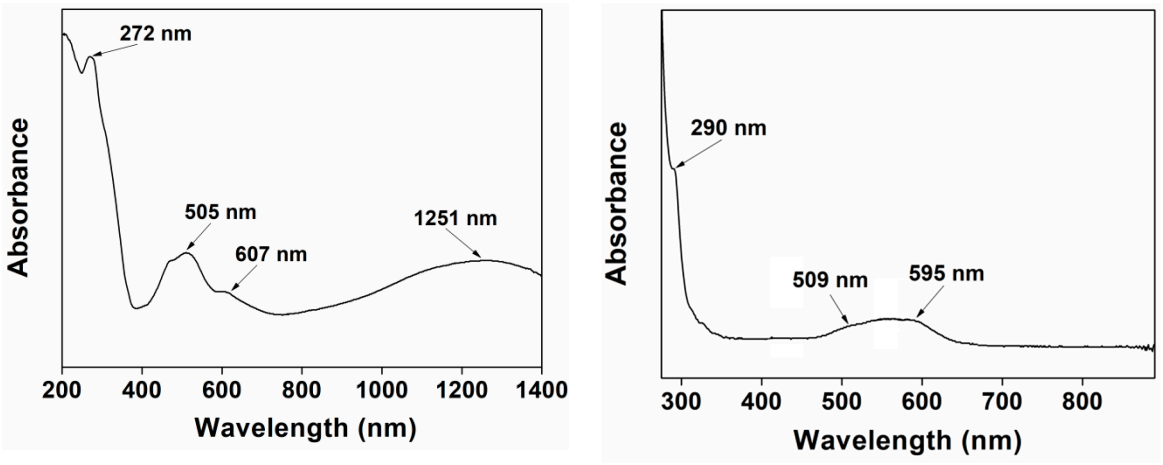

Figure S4. (**a**) UV-Vis-NIR spectrum of **2** (**b**) UV-Vis spectrum of **2**.

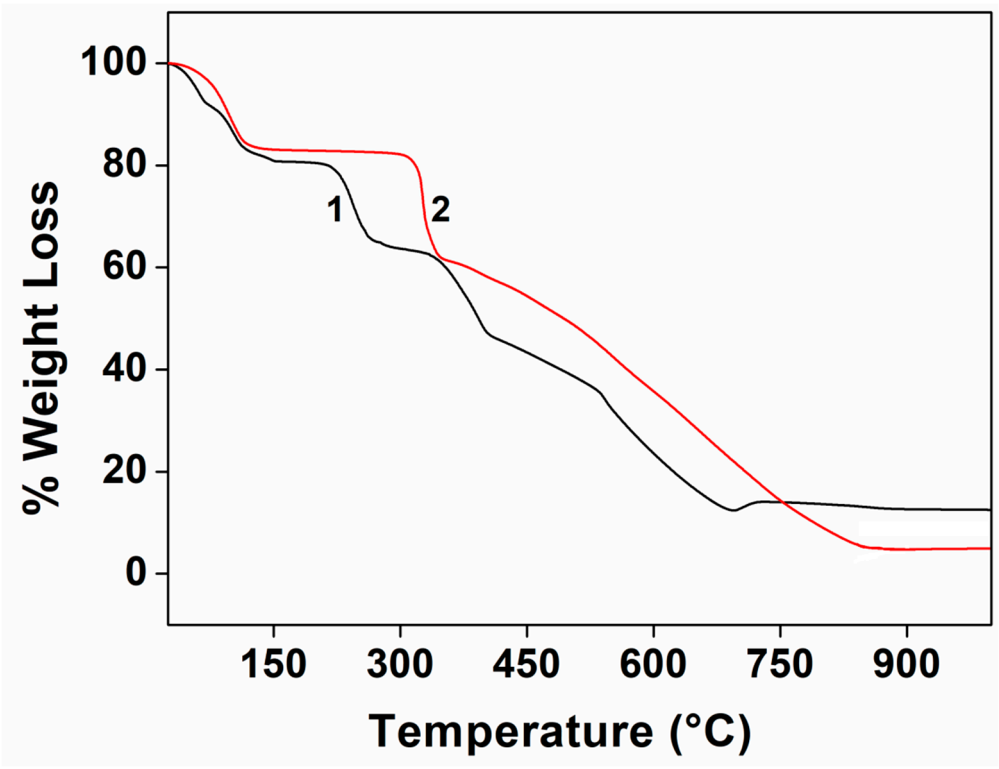

Figure S5. Thermogravimetric curves of the compounds **1** and **2**.

Supplementary references

1. Mautner, F.A.; Scherzer, M.; Berger, C.; Fischer, R.C.; Vicente, R.; Massoud, S.S. Synthesis and characterization of five new thiocyanato- and cyanato-metal(II) complexes with 4-azidopyridine as co-ligand. *Polyhedron* **2015,** *85,* 20–26.
2. Figgis, B. N.; Hitchman, M. A. *Ligand Field Theory and Its Applications;* Wiley-VCH: New York, **2000;** p 209.
3. Bruijnincx, P.C.A.; Sadler, P.J. New trends for metal complexes with anticancer activity. *Curr. Opin. Chem. Biol.* **2008,** *12,* 197–206.
4. Srinivasan, S.; Annaraj, J.; Athappan, P.R. Spectral and redox studies on mixed ligand complexes of cobalt (III) phenanthroline/bipyridyl and benzoylhydrazones, their DNA binding and antimicrobial activity. *J. Inorg. Biochem*. **2005,** *99,* 876–882.
5. Sharma, R.P.; Saini, A.; Singh, S.; Singh, A.; Venugopalan, P.; Ferretti, V. Second sphere coordination complexes: Synthesis, characterization, single crystal structure and packing analyses of [trans-$Cu(en)_2(H_2O)_2$]$(L_1/L_2)_2$ where L_1 = p-toluenesulphonate, L_2= 5-bromo-2-methoxybenzenesulphonate. *J. Mol. Struct.* **2010,** *69,* 155–162.

6. Batool, S.S.; Gilani, S.R.; Tahir, M.N.; Harrison, W.T.A.Z. Syntheses and Structures of Monomeric and Dimeric Ternary Complexes of Copper(II) with 2,2′-Bipyridyl and Carboxylate Ligands. *Anorg. Allg. Chem.* **2016,** *642,* 1364–1368.

7. Basumatary, D.; Lal, R. A.; Kumar, A. Synthesis, and characterization of low- and high-spin manganese(II) complexes of polyfunctional adipoyldihydrazone: Effect of coordination of N-donor ligands on stereo-redox chemistry. *J. Mol. Struct.* **2015,** *1092,* 122–129.

8. Gogoi, A.; Islam, S.M.N.; Frontera, A.; Bhattacharyya, M.K. Supramolecular association in Cu(II) and Co(II) coordination complexes of 3,5-dimethylpyrazole: Experimental and theoretical studies. *Inorg. Chim. Acta* **2019,** *484,* 133–141.

9. Dutta, D.; Islam, S.M.N.; Saha, U.; Frontera, A.; Bhattacharyya, M.K. Cu(II) and Co(II) coordination solids involving unconventional parallel nitrile(π)–nitrile(π) and energetically significant cooperative hydrogen bonding interactions: Experimental and theoretical studies. *J. Mol. Struct.* **2019,** *1195,* 733–743.